CDW-EIS calculations for multiple ionization of Ne, Ar, Kr and Xe by the impact of H$^+$ and

He$^+$, including post-collisional electron emission

CDW-EIS calculations for multiple ionization of Ne, Ar, Kr and Xe by the impact of H$^+$ and He$^+$, including post-collisional electron emission

C C Montanari[1,2], E C Montenegro[3] and J E Miraglia[1,2]

[1] Instituto de Astronomía y Física del Espacio, casilla de correo 67, sucursal 28, C1428EGA,
Buenos Aires, Argentina
[2] Departamento de Física, Facultad de Ciencias Exactas y Naturales, Universidad de Buenos Aires,
Buenos Aires, Argentina
[3] Instituto de Física, Universidade Federal de Rio de Janeiro, Caixa Postal 68528, Rio de Janeiro
21945-970, RJ, Brazil

E-mail: mclaudia@iafe.uba.ar

Abstract
We present theoretical single to quintuple ionization cross sections for Ne, Ar, Kr and Xe bombarded by H$^+$ and He$^+$. Post-collisional contributions due to Auger-like processes are taken into account using recent photoionization data. The present continuum distorted wave-eikonal initial state (CDW-EIS) and first Born approximation results are compared with the experimental data available in the energy range of 50–10 000 keV amu^{-1} for H$^+$ on Ne and Ar, and 50–1000 keV amu^{-1} for the other cases. In general, the combination of the CDW-EIS with the post-collisional branching ratios describes well the multiple ionization data above 300 keV amu^{-1}, showing a clear tendency to coalesce with the first Born approximation at high energies. The surprising result of this work is the good performance of the first Born approximation which describes rather well the experimental data of double and triple ionization, even in the intermediate energy range (50–300 keV amu^{-1}), where direct ionization is the dominant contribution.

(Some figures in this article are in colour only in the electronic version)

1. Introduction

Multiple ionization is a complex problem in atomic collisions, even more so when dealing with heavy targets [1]. There are many processes to be considered, such as direct multiple ionization, inner-shell ionization followed by post-collisional electron emission, like Auger, Coster–Krönig and shake-off processes [2–7], which often occur in succession generating a vacancy cascade and highly charged ions [8].

It has only recently been observed that the combination of the independent particle model with ratios of multi-charged ion production obtained from photoionization experiments leads to good results for multiple ionization in the MeV regime, where post-collisional electron emission plays a relevant role

[9–13]. However, the complexity of calculations within the independent electron model restricted the theoretical effort to Ne and Ar targets, while the experimental data go beyond the quadruple ionization of Xe. There are previous theoretical calculations for multiple ionization of Ne up to Xe but performed within the free-electron gas approximation [14].

The aim of this work is to present new continuum distorted wave-eikonal initial state (CDW-EIS) calculations for multiple ionization cross sections of Ne, Ar and, for the first time, Kr and Xe. The projectiles considered were protons and He$^+$. Furthermore, we include new results obtained within the first Born approximation and using the same potentials and numerical code.

J. Phys. B: At. Mol. Opt. Phys. **43** (2010) 165201

C C Montanari *et al*

The post-collisional ionization (PCI) or Auger-like process plays a major role in the final charge state distribution for projectile energies above 100 keV amu^{-1} for the Ar target and, for lower energies, for Kr and Xe targets. We take into account this contribution to the multiple ionization following Spranger and Kirchner [10], by using the branching ratios of charge state distributions from photoionization data.

The advent of attosecond physics caused time evolution of Auger relaxation processes in atoms and solids to attract increasing attention [15–17]. New measurements have been performed in the last 20 years using synchrotron radiation together with time-of-flight spectroscopy and coincidence techniques [18–31]. In this work we review photoionization branching ratios from the pioneering works by Carlson, Krause and co-workers [2–7] up to the present.

The work is organized as follows: in section 2 we present the theoretical developments for direct multiple ionization and for multiple ionization including PCI. We also include in this section a tabulation of the available branching ratios for Ne, Ar, Kr and Xe after single photoionization. In section 3, the results for single up to quintuple ionization of rare gases by H and He$^+$ are presented and compared with the experimental data available. Finally, the conclusions are drawn in section 4. Atomic units are employed throughout this work, except where specifically mentioned.

2. Theoretical developments

2.1. Direct multiple ionization

Within the independent particle model, the probability of direct ionization of exactly q_μ electrons of the μ-subshell (among a total of N_μ electrons in the subshell) is calculated by a binomial distribution of the single-ionization probabilities p_μ [1, 32] as follows:

$$P_\mu(q_\mu) = \binom{N_\mu}{q_\mu} p_\mu^{q_\mu}[1 - p_\mu]^{N_\mu - q_\mu}, \qquad (1)$$

where the probabilities $p_\mu = p_\mu(b, v)$ are the functions of the impact parameter b and the impact velocity v. Note that we use the Greek index μ to specify the quantum number of the initial state. We consider $\mu = $ 2p, 2s, 1s for Ne; $\mu = $ 3p, 3s, 2p, 2s for Ar; $\mu = $ 4p, 4s, 3d, 3p, 3s for Kr; and $\mu = $ 5p, 5s, 4d, 4p, 4s for Xe. Obviously, in all theses cases we have full shells so $N_{1s} = \cdots = N_{5s} = 2$; $N_{2p} = \cdots = N_{5p} = 6$; and $N_{3d} = N_{4d} = 10$.

If a total of i target electrons is ionized from the different subshells, $i = \sum_\mu q_\mu$, then the total probability of direct ionization of i electrons as a function of the impact parameter is the product

$$P_{(i)}(b, v) = \sum_{q_{1s}+q_{2s}+\cdots=i} \prod_\mu P_\mu(q_\mu). \qquad (2)$$

The main and more sensitive parameter within this multiple ionization formulation is the ionization probability $p_\mu(b, v)$. Different models are available in the literature to deal with its calculation, for example the time-dependent solution of the Schrödinger equation using the basis generator

method [10, 11, 33]; the CDW-EIS with Roothaan–Hartree–Fock orbitals and effective Coulomb continuum factors [12, 34]; or the semi-empirical exponential model [12]. All of them have been employed to describe multiple ionization of Ne and Ar. In this work, we calculate new and detailed ionization probabilities as the functions of the impact parameter for Ne, Ar, Kr and Xe by using the CDW-EIS and the first Born approximation as described next.

2.2. CDW-EIS and first Born calculations

We calculate the *T*-matrix elements following the same procedure as of previous papers [35, 36]. Summarizing, for each state characterized by the quantum numbers n and l, a target central potential is determined from the Hartree–Fock wavefunctions. The initial (bound) and final (continuum) electron wavefunctions are expanded in products of spherical harmonics and radial wavefunctions, obtained through the numerical solution of the radial Schrödinger equation [37]. To deal with dressed projectiles, we use an effective charge defined in terms of the momentum transfer extracted from the first Born approximation. This strategy has been successful in explaining the experiments of total ionization cross sections [38].

It is convenient to expand the *T*-matrix element for a given angle (Ω), energy (E) of the ejected electron and momentum transfer ($\overrightarrow{\eta} = \{\eta, \varphi_\eta\}$) as follows:

$$T(E, \Omega, \overrightarrow{\eta}) = \sum_{m=-M}^{M} i^m \frac{\exp(im\,\varphi_\eta)}{\sqrt{2\pi}} T_m(E, \Omega, \eta). \qquad (3)$$

We integrate numerically the matrix elements for different angular momenta and add them appropriately. To be consistent, the maximum value M was considered to be the maximum angular momentum used to solve the Schrödinger equation. For practical purposes, all these $T_m(E, \Omega, \eta)$ values are stored in a large table of $(2 \times 8 + 1)$ to $(2 \times 32 + 1)$ values of m, around 70 values of η, 28 angles, and between 33 and 45 values of E for a given initial state with the quantum numbers n, l and m.

Using equation (3) we can calculate the transition amplitudes as a function of the impact parameter $\overrightarrow{b}$ with the help of the two-dimensional Fourier transform

$$a(E, \Omega, \overrightarrow{b}) = \int d\overrightarrow{\eta}\, \frac{\exp(i\,\overrightarrow{b} \cdot \overrightarrow{\eta})}{2\pi} T(E, \Omega, \overrightarrow{\eta}). \qquad (4)$$

After some simple algebra, equation (4) can be written as

$$a(E, \Omega, \overrightarrow{b}) = \sum_{m=-M}^{M} i^m \frac{\exp(im\,\varphi_b)}{\sqrt{2\pi}} a_m(E, \Omega, b), \qquad (5)$$

with

$$a_m(E, \Omega, b) = i^{-m} \int_0^\infty \eta\, d\eta\, J_m(b\eta) T_m(E, \Omega, \eta), \qquad (6)$$

and $J_m(b\eta)$ being the cylindrical Bessel function. The total probability to be used in the binomial forms is obtained after integrating in the ejected-electron space:

$$p(\overrightarrow{b}) = \int dE \int d\Omega |a(E, \Omega, \overrightarrow{b})|^2$$

$$= \frac{1}{2\pi} \sum_{m=-M}^{M} \int dE \int d\Omega |a_m(E, \Omega, b)|^2. \qquad (7)$$

It is convenient to recalculate the total cross section as $\sigma = \int d\vec{b}\ p(\vec{b})$ to check the calculation. At most, differences of very few per cent are observed when compared with the total cross section integrating directly on $\vec{\eta}$.

In order to achieve convergent results we include very large impact parameters. For instance, for the outer shells we need to consider impact parameters as large as 60 au. The CDW-EIS and Born approximation were calculated on an equal footing.

As usual, total cross sections are calculated involving the sum over all the relevant states of the target. In this work we extend it to include two complete shells: i.e. for Ne ($nlm = 2p_{0\pm1}$, 2s and 1s), Ar ($3p_{0\pm1}$, 3s, $2p_{0\pm1}$ and 2s), Kr ($4p_{0\pm1}$, 4s, $3d_{0\pm1\pm2}$, $3p_{0\pm1}$ and 3s) and Xe ($5p_{0\pm1}$, 5s, $4d_{0\pm1\pm2}$, $4p_{0\pm1}$ and 4s). The CDW-EIS calculations require a huge amount of computing time—about a few months—in our small cluster.

2.3. Multiple ionization including PCI

The PCI, as a generalization of all the time-delayed electron emission processes, is essentially independent of the nature of the primary ionization event [1], and can be considered separately. It is present not only in atomic targets [9–12, 14] but also in collisions with molecules [39, 40].

As noted by Cavalcanti and co-workers [9], for high impact energies, the experimental data for multiple ionization cross sections show almost the same slope as the single one [41, 42]. Moreover, for Kr and Xe the measurements of triple and quadruple ionization cross sections around 1 MeV are two orders of magnitude above the theoretical estimations for direct ionization by the multinomial expression (2). These facts reveal the importance of PCI in the multiple ionization at high energies [13].

If $F_{\mu,k}$ is the branching ratio of single ionization of a certain μ-subshell followed by PCI of k electrons of the outer shells (Auger cascades), ending with an ion charge state $k+1$, then

$$\sum_{k=0}^{k_{max}} F_{\mu,k} = 1. \tag{8}$$

The maximum number of post-collisional emitted electrons, k_{max}, depends on the initial single-ionization state.

The term $p_\mu^{q_\mu}$ of equation (1) can be written as follows:

$$p_\mu^{q_\mu} = (p_\mu \times 1)^{q_\mu} = \left(p_\mu \times \sum_{k=0}^{k_{max}} F_{\mu,k} \right)^{q_\mu}. \tag{9}$$

Replacing (9) in (1), the probability of direct multiple ionization of q_μ electrons from the μ-subshell can be rewritten as

$$P_\mu(q_\mu) = \binom{N_\mu}{q_\mu} \left[p_\mu \sum_{k=0}^{k_{max}} F_{\mu,k} \right]^{q_\mu} [1 - p_\mu]^{N\mu - q_\mu}$$
$$= P_\mu(q_\mu) \left[\sum_{k=0}^{k_{max}} F_{\mu,k} \right]^{q_j}. \tag{10}$$

The final number of the emitted electrons, considering direct ionization plus PCI, varies from q_μ ($k = 0$, no Auger emission)

up to $q_\mu + k_{max}$. The expansion and rearrangement of equation (10), in order to put together those terms which contribute to the same number of final emitted electrons, gives

$$P_\mu(q_\mu) = \sum_{k=0}^{k_{max}} P'_\mu(q_\mu, k). \tag{11}$$

We can interpret $P'_\mu(q_\mu, k)$ as the probability of direct ionization of q_μ electrons followed by PCI of k more electrons, so that finally $\alpha_\mu = q_\mu + k$ electrons are emitted. For $q_\mu = 1$

$$P'_\mu(1, k) = P_\mu(1)\ F_{\mu,k}. \tag{12}$$

For $q_\mu > 1$, the first four $P'_\mu(q_\mu, k)$ are

$$\begin{cases} P'_\mu(q_\mu, 0) = P_\mu(q_\mu)\binom{q_\mu}{0}[F_{\mu,0}]^{q_\mu} \text{ (no Auger-like emission)}, \\ P'_\mu(q_\mu, 1) = P_\mu(q_\mu)\binom{q_\mu}{1}[\ F_{\mu,0}]^{q_\mu - 1} F_{\mu,1}, \\ P'_\mu(q_\mu, 2) = P_\mu(q_\mu)\left\{\binom{q_\mu}{1}[F_{\mu,0}]^{q_\mu - 1} F_{\mu,2} \right. \\ \qquad\qquad \left. + \binom{q_\mu}{2}[F_{\mu,0}]^{q_\mu - 2}[F_{\mu,1}]^2 \right\}, \\ P'_\mu(q_\mu, 3) = P_\mu(q_j)\ \left\{\binom{q_\mu}{1}[F_{\mu,0}]^{q_\mu - 1} F_{\mu,3} \right. \\ \qquad\qquad + 2\binom{q_\mu}{q_\mu - 2}[F_{\mu,0}]^{q_\mu - 2} F_{\mu,1} F_{\mu,2} \\ \qquad\qquad \left. + \binom{q_\mu}{3}[F_{\mu,0}]^{q_\mu - 3}[F_{\mu,1}]^3 H(q_\mu - 2) \right\}, \end{cases} \tag{13}$$

with $H(x)$ being the Heaviside function, so that the third term in $P'_\mu(q_\mu, 3)$ only appears for $q_\mu > 2$.

Then, the probability $\wp_\mu^{PCI}(\alpha_\mu)$ of emission of α_μ electrons, no matter how many electrons come from direct ionization of the μ-subshell and how many electrons are emitted by PCI, will be the addition of $P'_\mu(q_\mu, k)$, so that $q_\mu + k = \alpha_\mu$. In general,

$$\wp_\mu^{PCI}(\alpha_\mu) = P'_\mu(\alpha_\mu, 0) + P'_\mu(\alpha_\mu - 1, 1)$$
$$+ P'_\mu(\alpha_\mu - 2, 2) + \cdots + P'_\mu(1, \alpha_\mu - 1), \tag{14}$$

with $P'_\mu(\alpha_\mu, k)$ being those of equation (13). In this way, the single- up to triple-ionization probabilities including PCI, $\wp_\mu^{PCI}(\alpha_\mu)$, are

$$\begin{cases} \wp_\mu^{PCI}(1) = P_\mu(1)\ F_{\mu,0}, \\ \wp_\mu^{PCI}(2) = P_\mu(1)\ F_{\mu,1} + P_\mu(2)[F_{\mu,0}]^2, \\ \wp_\mu^{PCI}(3) = P_\mu(1)F_{\mu,2} + 2P_\mu(2)F_{\mu,0}F_{\mu,1} + P_\mu(3)[F_{\mu,0}]^3. \end{cases} \tag{15}$$

Finally, if we replace $P_\mu(q_\mu)$ by $\wp_\mu^{PCI}(\alpha_\mu)$ in equation (2), we obtain the total probability of multiple ionization of i electrons, including PCI, as follows:

$$P_{(i)}^{PCI}(b, v) = \sum_{\alpha_{1s} + \alpha_{2s} + \cdots = i} \prod_\mu \wp_\mu^{PCI}(\alpha_\mu). \tag{16}$$

As the method employed is unitarized, the following closure relations hold:

$$\sum_{q_\mu=1}^{N_\mu} P_\mu(q_\mu) = \sum_{\alpha_\mu=1}^{\alpha_{\mu max}} \wp_\mu^{PCI}(\alpha_\mu) \tag{17}$$

and

$$\sum_{i=1} P_{(i)}(b, v) = \sum_{i=1} P_{(i)}^{PCI}(b, v). \tag{18}$$

Table 1. Compilation of experimental [2–7, 18–28] and calculated [43, 47] photoionization branching ratios. $F_{\mu,i}$ is the yield of single photoionization of the μ-subshell followed by the post-collisional emission of i electrons from the outer shells, with the final charge state being $i + 1$.

Ne

	1s[a]	1s[b]	1s[c]	1s[d]	1s[e]	K-L[e,f]	2s[d,g]	L-shell[f,h]
$F_{\mu,0}$	**0.0193**	0.015	0.000	0.013	0.00	0.010	**1.00**	0.873
$F_{\mu,1}$	**0.921**	0.935	0.939	0.980	0.921	0.736	**0.00**	0.119
$F_{\mu,2}$	**0.0571**	0.048	0.058	0.007	0.075	0.22	**0.00**	0.008
$F_{\mu,3}$	**0.0028**	0.003	0.003	0.000	0.004	0.031	**0.00**	0.000
$F_{\mu,4}$	**0.000**	0.000	0.000	0.000	0.000	0.01	**0.00**	0.000

Ar

	2s[k]	2s[u]	2s[f]	2p[k,v]	2p[u]	2p[f]	3s[k,u]	M-shell[f]
$F_{\mu,0}$	**0.000**	0.000	0.00	**0.005**	0.00	0.00	**1.00**	0.855
$F_{\mu,1}$	**0.010**	0.023	0.02	**0.863**	0.87	0.74	**0.00**	0.135
$F_{\mu,2}$	**0.890**	0.860	0.72	**0.128**	0.12	0.24	**0.00**	0.01
$F_{\mu,3}$	**0.100**	0.110	0.24	**0.003**	0.01	0.02	**0.00**	0.00
$F_{\mu,4}$	**0.000**	0.000	0.02	**0.001**	0.00	0.00	**0.00**	0.00

Kr

	3s[l]	3s[m]	3p[l]	3p[n]	3p[k]	3p[m]	3d[l]	3d[k]	3d[m]	4s[l,m]
$F_{\mu,0}$	**0.00**	0.000	**0.00**	0.000	0.000	0.000	**0.005**	< 0.01	0.00	**1.00**
$F_{\mu,1}$	**0.01**	0.152	**0.02**	0.035	0.030	0.10	**0.670**	0.70	0.69	**0.00**
$F_{\mu,2}$	**0.12**	0.465	**0.60**	0.586	0.635	0.45	**0.320**	0.30	0.31	**0.00**
$F_{\mu,3}$	**0.66**	0.273	**0.36**	0.326	0.335	0.45	**0.005**	0.00	0.00	**0.00**
$F_{\mu,4}$	**0.21**	0.110	**0.02**	0.052	0.000	0.00	**0.00**	0.00	0.00	**0.00**

Xe

	4s[p]	4p[q]	4p[p]	4d[r]	4d[s]	4d[p]	N-shell[f]	5s[t]
$F_{\mu,0}$	**0.00**	**0.00**	0.00	**0.00**	< 0.01	0.000	0.050	**1.00**
$F_{\mu,1}$	**0.01**	**0.05**	0.036	**0.80**	0.80	0.997	0.400	**0.00**
$F_{\mu,2}$	**0.165**	**0.89**	0.913	**0.20**	0.19	0.003	0.280	**0.00**
$F_{\mu,3}$	**0.774**	**0.06**	0.051	**0.00**	0.00	0.000	0.210	**0.00**
$F_{\mu,4}$	**0.051**	**0.00**	0.00	**0.00**	0.00	0.000	0.048	**0.00**

For Ne: [a]Landers et al [18]; [b]Morgan et al [19]; [c]Saito et al [20], corrected to exclude L-shell ionization; [d]Kochur et al [43]; [e]Carlson et al [2], corrected to exclude L-shell ionization; [f]Carlson et al [3], K–L initial vacancy; [g]Krause et al [4]; [h]Carlson et al [5], photon energy just above the K-shell ionization threshold.
For Ar: [k]Brünken et al [21]; [u]Carlson et al [6]; [v]Viefhaus et al [22]; [f]Carlson et al [3], photon energy just above the L-shell ionization threshold.
For Kr: [l]Tamenori et al [23]; [m]Krause et al [7]; [n]Armen et al [24]; [k]Brünken et al [21].
For Xe: [p]Kochur et al [47], theoretical calculation; [q]Hikosaka et al [25]; [r]Hayaishi et al [26]; [s]Kämmerling et al [27]; [f]Carlson et al [3], includes O-shell ionization; [t]Hayaishi et al [28].

2.4. Branching ratios of the charge-state distribution after photoionization

Production of multiple-charged ions by cascades of de-excitations following direct photoionization of inner-shells has been studied both experimentally and theoretically [43]. In the early works by Carlson, Krause and co-workers, the initial inner-shell vacancies were produced with x-ray tubes [2–7]. A new wave of interest in the problem of multiple-charged ion production has arisen in the last few years with the advent of new experimental techniques for photoionization research [44–46].

Pioneered by Krause et al [4], the photoelectron–ion as well as Auger-electron–ion coincidence measurements permit us to accurately determine the total yield of Auger-electron emission processes for vacancies in different shells of various atoms [44], and to exclude multiple ionization upon creation of an initial vacancy. Results are obtained in coincidence between the photoelectron lines and slow electrons in the 0–30 eV kinetic energy range [30].

In table 1, we present a rather complete compilation of different experimental branching ratios, $F_{\mu,i}$ of equation (8), for Ne, Ar, Kr and Xe due to an initial single vacancy in the μ-subshell. The vertical sum of each column is equal to 1. In this work, we use the ratios indicated with bold numbers in table 1.

Auger emission in these targets is energetically possible for initial vacancies from the deepest to the subvalence shells [43]. This fact, already mentioned by Krause and Carlson [4, 6] and Saito et al [20], is expressed in table 1 in the columns 2s for Ne, 3s for Ar, 4s for Kr and 5s for Xe with $F_{\mu,i} = \delta_{i,0}$ (meaning that single ionization of these shells does not contribute to PCI [4, 6, 7, 21, 23, 28, 43]).

This is an important point because in recent works [9, 10, 12, 42], the PCI of Ne and Ar targets were included by using the experimental data of table IV by Carlson *et al* [3]. These values represent the charge-state distribution after photoabsortion of x-rays with energies chosen in order to determine the shell that dominates the vacancy production; however, photoabsortion can take place in any shell whose binding energy is smaller than the x-ray energy. Moreover, in previous works, Carlson, Krause and co-workers published their measurements corrected to exclude outer-shell ionization ([2] for Ne, [6] for Ar, [7] for Kr). For instance, K-shell photoionization of Ne includes K- and L-shell ionization. The measurements by Carlson and Krause appear in both columns 6 and 7 of table 1, but in column 6 they are corrected to exclude L-shell ionization. Note that these corrected values for 1s single photoionization of Ne by Krause *et al* [2] in the 1960s are in very good agreement with the most recent ones by Landers *et al* [18] using COLTRIMS techniques.

The values displayed in column 9 of table 1 for Ne L-shell ionization correspond to 850 eV x-ray energy (just below the K-shell binding energy) and not to PCI after a 2s single vacancy. As expressed by Krause and Carlson [4], the filling of a 2s hole by the Auger process is difficult to defend as it is endothermic. The first and second ionization potentials for Ne are 21.6 and 40.9 eV, respectively, so these ratios may include 2s and 2p multiple initial vacancies or PCI following 1s photoexcitation of Ne to a Rydberg state [48].

The same arguments are valid for Ar: the values displayed in column 9 of table 1 for M-shell ionization correspond to measurements with a photon energy just below the L-shell ionization threshold and not to Auger after the creation of a single 3s hole [3, 6].

In summary, the values of Carlson that should be used combined with direct ionization calculations for Ne and Ar are those in table 1 with the superscripts *d*, *g* and *u* [2, 4, 6] instead of *f* [3].

3. Results and discussion

We compare in figure 1 our CDW-EIS and Born results for direct multiple ionization cross sections of Ne by H$^+$ and He$^+$, with the theoretical curves by Kirchner and co-workers [10, 33], and by Galassi *et al* [12] in the energy region between 40 and 1000 keV amu^{-1}. To make the comparison among these calculations clearer, we have not considered any PCI in the results shown in this figure. All these curves are obtained within the independent electron model and employ the same binomial distribution for the direct multiple ionization as given by equation (2). We also include in this figure the experimental data by Cavalcanti *et al* [41] and DuBois [49].

We can observe in figure 1 that the theoretical results agree rather well for single ionization, but the differences among them become larger as the ionization level increases from single to triple or quadruple ionization, showing that the calculations are very sensitive to the impact-parameter dependence.

Figures 2–9 summarize the main results of this work. We display in these figures multiple ionization cross sections
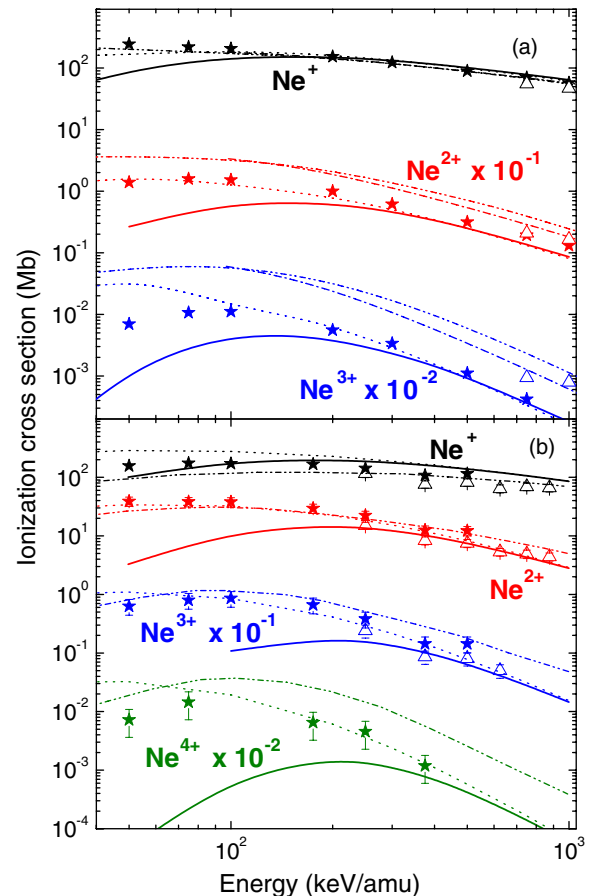

Figure 1. Multiple ionization cross section of Ne by H$^+$ (a) and He$^+$ (b). The theoretical results consider only direct processes without PCI contributions. (a) Curves: —— CDW-EIS; · · · · · · Born; — · — Galassi *et al* [12]; — · · — Spranger *et al* [10]; experimental data: △, Cavalcanti *et al* [9]; ★, DuBois *et al* [49]. (b) Curves: —— CDW-EIS; · · · · · · Born; — · · — Kirchner *et al* [33]; experimental data: △, Santos *et al* [53]; ★, DuBois *et al* [50].

(single to quintuple) of Ne, Ar, Kr and Xe, by the protons and He$^+$(1s) impact, calculated with the CDW-EIS and the first Born approximations. These calculations were performed for direct multiple ionization, using equation (2), and for total multiple ionization including PCI, using equation (16), so that two curves (with and without PCI) are displayed in each case. No electron transfer processes are included.

In all the figures, the theoretical curves are compared with the available experimental data. In general, we performed calculations in the energy range from 50 to 1000 keV amu^{-1}, because there are no experimental cross sections available for higher energies. The exceptions are the cases of H$^+$ in Ne and Ar, for which we have extended calculations with the first Born approximation up to 10 MeV.

As mentioned in section 2.4, multiple ionization cross sections including PCI have been obtained by using the ratios in table 1 indicated with bold numbers. As can be observed in this table, the branching ratios that correspond to single photoionization measurements are quite similar, and the differences in the total cross sections by using different sets of values are small.
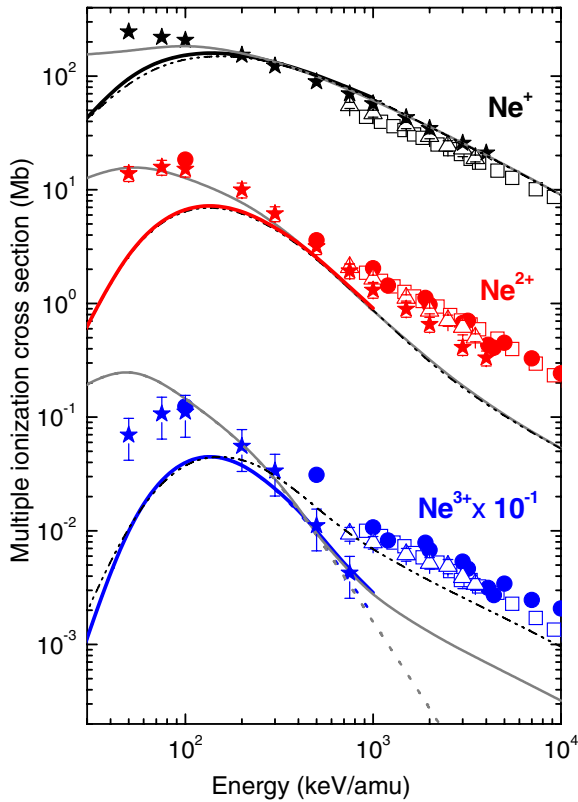
J. Phys. B: At. Mol. Opt. Phys. **43** (2010) 165201

C C Montanari *et al*

Figure 2. Single (Ne⁺), double (Ne²⁺) and triple (Ne³⁺) ionization cross sections of neon by the proton impact. Curves: thick-lines, CDW-EIS results with (——) and without (······) PCI; thin grey lines, Born results with (——) and without (······) PCI; dash-double-dotted lines, CDW-EIS including PCI after 2s initial vacancy [3]. Experimental data: △, Cavalcanti *et al* [9]; ★, DuBois *et al* [49]; ●, Andersen *et al* [51]; □, electron-impact data by Schram *et al* [52].

3.1. Neon

Figures 2 and 3 show our theoretical results for the H⁺ and He⁺ impact on Ne, respectively. In figure 2 we display only single to triple ionization cross sections, because no experimental results were found in the literature for higher ionization states. For He⁺ on Ne, in figure 3, the quadruple ionization measurements by DuBois [50] are also included. Curiously, the first Born approximation describes very well the multiple ionization of Ne by protons, being even better for the He⁺ impact. The CDW-EIS describes single ionization better than the Born approximation, but the multiple ionization results underestimate the data for the lowest energies considered, and get closer to the Born calculations for energies above 500 keV amu⁻¹.

It can be observed in figures 2 and 3 that the separation between the results with and without PCI (solid and dotted lines) is very small for single and double ionization, but begins to be noticeable for triple ionization at impact energies above 500 keV amu⁻¹, where the K-shell ionization starts to be significant.

In the case of H⁺ on Ne, shown in figure 2, the theoretical description underestimates the data for double and triple ionization above 1 MeV. In previous works [9, 10, 12], the values from Carlson *et al* [3] for ion charge states after
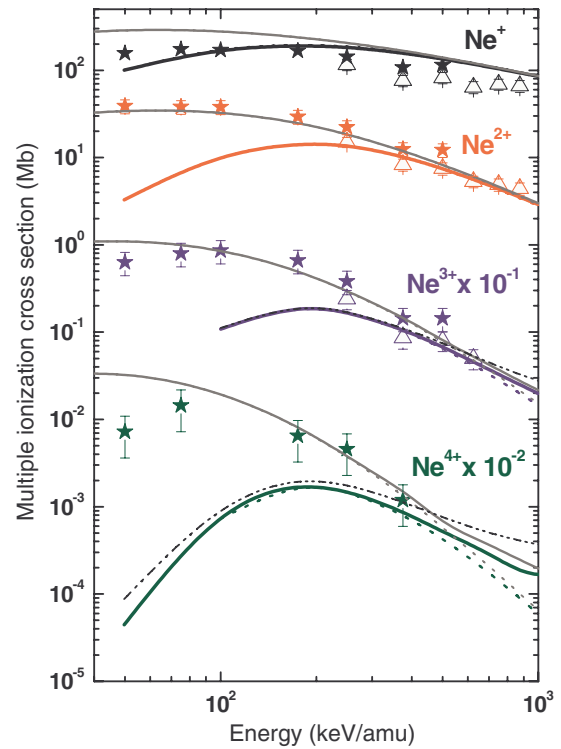

Figure 3. Single (Ne⁺), double (Ne²⁺), triple (Ne³⁺) and quadruple (Ne⁴⁺) ionization cross sections of Neon by the He⁺(1s) impact. Curves as in figure 2. Experimental data: △, Santos *et al* [53]; ★, DuBois *et al* [50].
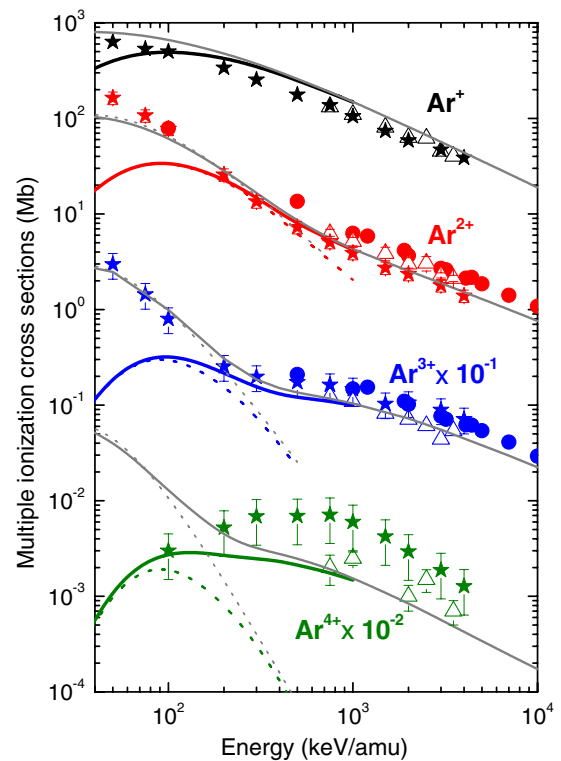

Figure 4. Single (Ar⁺), double (Ar²⁺), triple (Ar³⁺) and quadruple (Ar⁴⁺) ionization cross sections of argon by the proton impact. Curves as in figure 2. Experimental data: △, Cavalcanti *et al* [9]; ★, DuBois *et al* [49]; ●, Andersen *et al* [51]. Also included electron-impact data: □, McCallion *et al* [54]; and +, Syage [55].
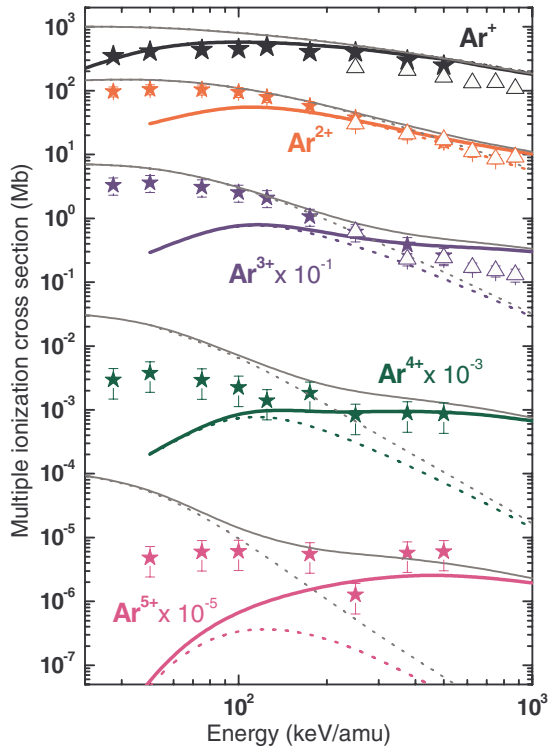
Figure 5. Single (Ar^+), double (Ar^{2+}), triple (Ar^{3+}), quadruple (Ar^{4+}) and quintuple (Ar^{5+}) ionization cross sections of argon by the $He^+(1s)$ impact. Curves as in figure 2. Experimental data as in figure 6.
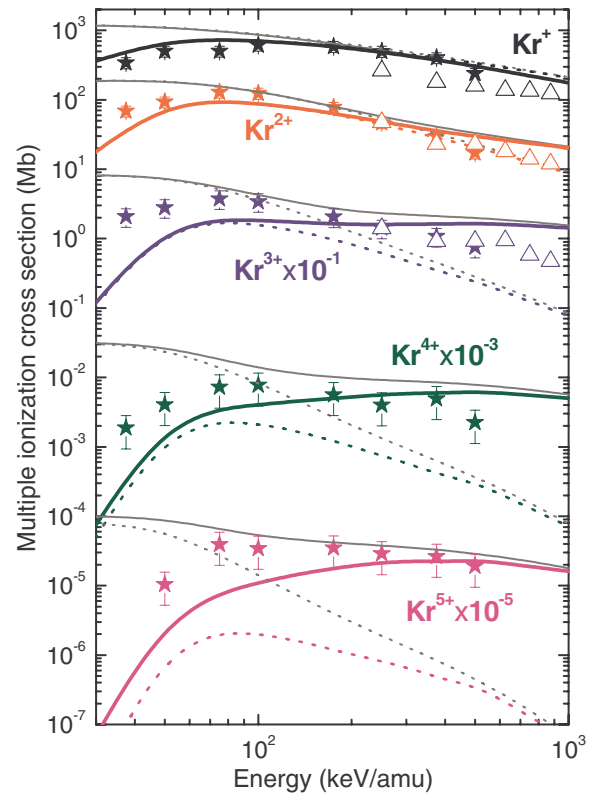

Figure 7. Single (Kr^+), double (Kr^{2+}), triple (Kr^{3+}), quadruple (Kr^{4+}) and quintuple (Kr^{5+}) ionization cross sections of krypton by the $He^+(1s)$ impact. Curves as in figure 2. Experimental data as in figure 6.
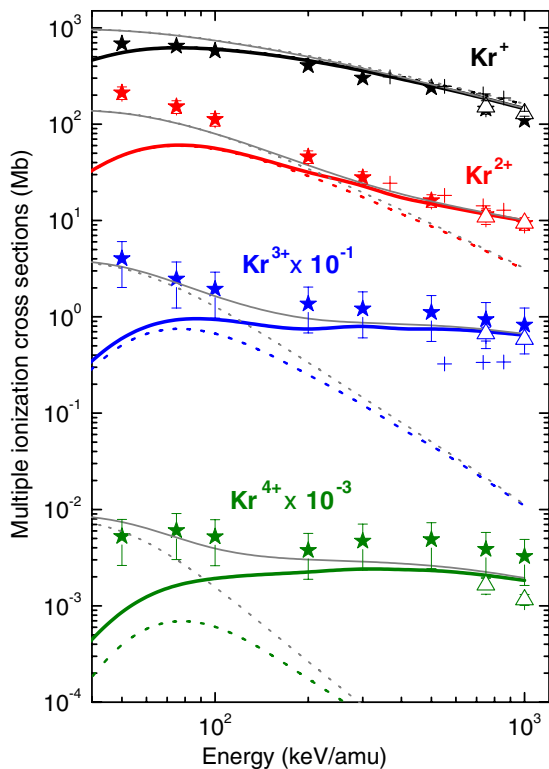
photoionization of the L-shell were interpreted as rates of Auger emission after single vacancy in the 2s-subshell. But, as mentioned in section 2.4, no Auger decay is expected to occur after single vacancy of the 2s-subshell [2, 4, 20, 43].

If we perform the multiple ionization calculation combining our present CDW-EIS with the ratios of Auger emission shown in column 9 of table 1 (possible 2s contribution to PCI), instead of column 8 (no PCI after 2s single ionization), the triple ionization results agree well with most of the experimental data (Cavalcanti *et al* [41], Andersen *et al* [51] and Schram *et al* [52]). However, the same ratios do not change the double ionization cross sections.

These results indicate that the theoretical description of double and triple ionization of Ne at high energies requires improvement related to multiple-ionization channels not considered here as, for example, the K-shell excitation followed by outer-shell ionization, i.e. PCI of Ne $1s^{-1}3p$ and Ne $1s^{-1}4p$ due to resonant Auger shake-off decay, or Auger decay followed by autoionization [48].

3.2. Argon

Single to quintuple ionization of Ar by the H^+ and He^+ impact from intermediate to high energies were calculated with the CDW-EIS and first Born approximation. In figures 4 and 5, we include the corresponding theoretical curves compared with the available experimental data.
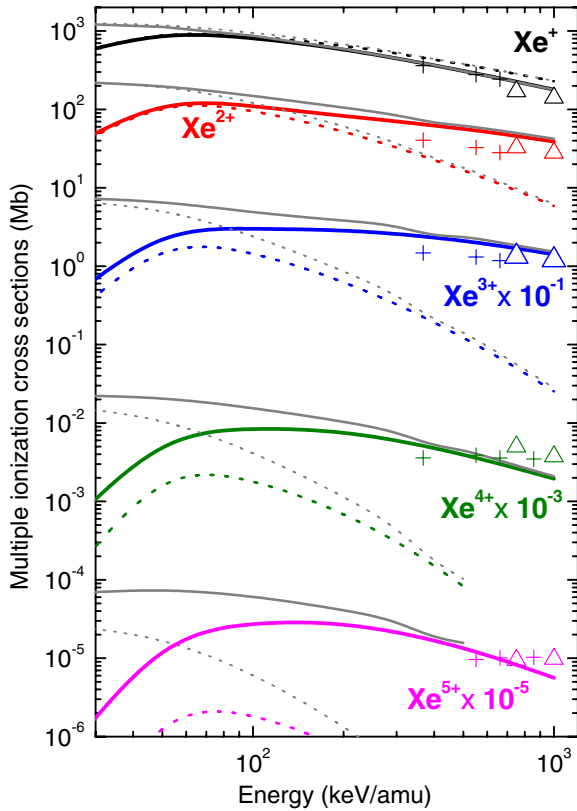

Figure 6. Single (Kr^+), double (Kr^{2+}), triple (Kr^{3+}) and quadruple (Kr^{4+}) ionization cross sections of krypton by the proton impact. Curves as in figure 2. Experimental data: △, Cavalcanti *et al* [9]; ★, DuBois *et al* [49]; +, electron-impact data by Syage [55].

Figure 8. Single (Xe^+), double (Xe^{2+}), triple (Xe^{3+}), quadruple (Xe^{4+}) and quintuple (Xe^{5+}) ionization cross sections of xenon by the proton impact. Curves as in figure 2. Experimental data: $\triangle$, Cavalcanti *et al* [9] and + Syage [55] for the electron impact.

Figure 9. Single (Xe^+), double (Xe^{2+}), triple (Xe^{3+}), quadruple (Xe^{4+}) and quintuple (Xe^{5+}) ionization cross sections of xenon by the $He^+(1s)$ impact. Curves as in figure 2. Experimental data: $\triangle$, Santos *et al* [53].

Again, the CDW-EIS results converge to the Born ones for the highest energies considered and underestimate the data for the lowest ones. The first Born results for double and triple ionization provide surprisingly good agreement with the experiment within the whole energy range. For quadruple and quintuple ionization, this good agreement occurs only for impact energies above 200 keV amu^{-1}.

The CDW-EIS shows very good results for single ionization in the whole energy range of figures 4 and 5, and above 200 keV amu^{-1} for double and triple ionization. It can also be observed that the CDW-EIS describes better than the Born approximation the experimental data for quadruple ionization.

The influence of the PCI in these results can be seen in both figures by comparing the differences between the solid and dotted curves. The change in the slopes of the curves at high velocities, following the tendency of the experimental data, shows that the method described in section 2.3 is a good approximation for the inclusion of the PCI to the direct multiple ionization. For instance, for the proton-impact case at 1 MeV, triple ionization with PCI is one order of magnitude larger than direct triple ionization, this factor becoming even larger for quadruple and quintuple ionization. This enhancement is due to the contribution from Auger emission after single ionization of the L-shell. Multiple ionization is a test of the theoretical description for the inner-shell ionization. The higher the final charge state, the deeper the dominant shell.
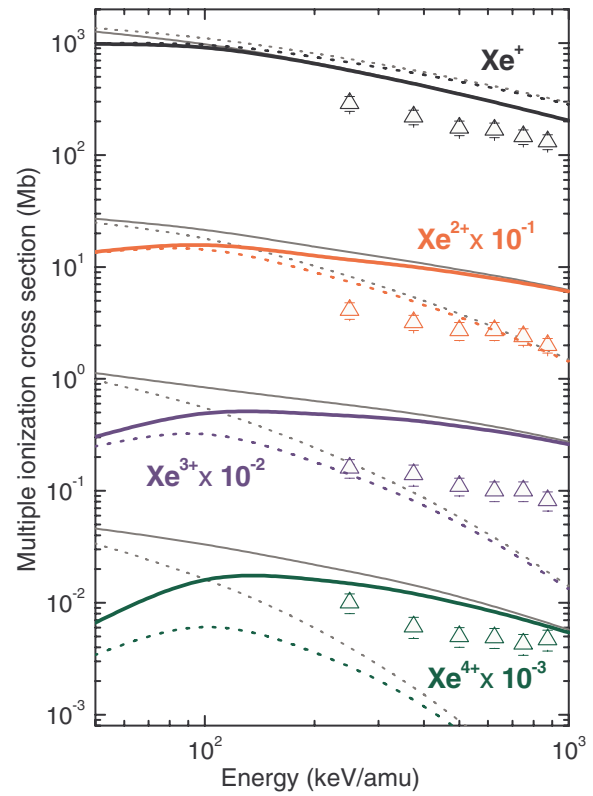
3.3. Krypton

Figures 6 and 7 show two of the main results of this work. They show the first theoretical calculation of multiple ionization of Kr by H^+ and He^+. These figures reproduce well the experimental measurements of two groups, DuBois *et al* [49, 50] and Montenegro and collaborators [9, 53]. We also include in figure 6 the electron-impact results from [55] at high velocities. We can observe that the first Born approximation results, displayed in figure 6, are again in very good agreement with the experiment even for the quadruple ionization.

For He^+ in Kr, in figure 7, the CDW-EIS curves agree better than the Born approximation with the experimental data, following the experimental tendency for low energies, up to 40 keV amu^{-1}. In this case, we also show the quintuple ionization cross sections, which agree with DuBois [50] measurements.

Both theoretical curves converge at high energies, with (solid lines) or without (dotted lines) PCI. These high-energy values (above 500 keV amu^{-1}) agree quite well with the experimental data for the H^+ impact [9, 49], but for the He^+ impact above 700 keV amu^{-1} they overestimate the data by Santos *et al* [53].

3.4. Xenon

Multiple ionization of Xe is also theoretically described for the first time. In figure 8 we show our results from

single to quintuple ionization cross sections of protons in Xe. To our knowledge, only Cavalvanti *et al* [41] measured multiple ionization of Xe by protons, and for energies above 750 keV amu^{-1}. We also include in this figure the data by Syage [55] for the electron-impact energy above 200 eV. No experimental data exist in the literature for lower energies.

The theoretical description of the data is very good for both models, first Born approximation and CDW-EIS. The experimental values are in the energy region where both curves converge, and are very well described from single up to quintuple ionization.

In figure 9 we display our theoretical results for He$^+$ on Xe together with the experimental data by Santos *et al* [53]. The curves seem to follow qualitatively the slopes of the data, but the differences are a factor 2 for single and quadruple ionization and a factor 3 for double and triple ionization. For He$^+$ on Xe, neither Born nor CDW-EIS can explain the experimental results as has been observed for the H$^+$ impact in Xe, or with the good agreement shown for the other collisional systems considered here.

4. Conclusions

In this work we present CDW-EIS and first Born approximation calculations for multiple ionization of Ne and Ar, and, for the first time, of Kr and Xe up to quintuple ionization. Direct and PCI processes were included. In the case of the direct ionization, the usual multichannel distribution has been employed, while, for PCI, the rearrangement of the multinomial distribution has been considered by using experimental ratios of the final charge-state distribution.

The agreement between our calculations and the experimental data is in general very good, especially for Ar and Kr targets for both H$^+$ and He$^+$ ions. In the case of H$^+$ in Xe, and He$^+$ in Ar and Kr, up to quintuple ionization cross sections were calculated and the agreement between theory and experiments is also very good. A curious, and probably fortuitous, result of our calculations is the good performance of the first Born approximation for all the collisional systems. Although this approximation fails when dealing with single ionization, it provides a very good description of multiple ionization even for energies between 50 and 300 keV amu^{-1}, and, of course, for higher energies, where it coalesces with the CDW-EIS.

Two cases need further work both experimentally and theoretically: the underestimation of the experimental data for double and triple ionization of Ne by protons, and the systematic differences between theory and experiment in the multiple ionization of Xe by He$^+$, not found in the other cases. For the case of H$^+$ in Ne, the underestimation in the high-energy region, where PCI is very important, reveals the presence of post-collisional emission channels not included in the calculations, as for example, the PCI after Ne K-shell excitation to Rydberg states. Studies to include this contribution are underway by our group.

References

[1] DuBois R D and Manson S T 1987 *Phys. Rev.* A **35** 2007
[2] Carlson T A and Krause M O 1965 *Phys. Rev.* **140** A1057
[3] Carlson T A, Hunt W E and Krause M O 1966 *Phys. Rev.* **151** 41
[4] Krause M O, Vestal M V, Johnson W H and Carlson T A 1964 *Phys. Rev.* **133** A385
[5] Carlson T A and Krause M O 1965 *Phys. Rev. Lett.* **14** 390
[6] Carlson T A and Krause M O 1965 *Phys. Rev.* **137** A1655
[7] Krause M O and Carlson T A 1966 *Phys. Rev.* **149** 52
[8] Morishita Y, Tamenori Y, Okada K, Oyama T, Yamamoto K, Tabayashi K, Ibuki T, Moribayashi K and Suzuki I H 2006 *J. Phys. B: At. Mol. Opt. Phys.* **39** 1323
[9] Cavalcanti E G, Sigaud G M, Montenegro E C, Sant'Anna M M and Schmidt-Bocking H 2002 *J. Phys. B: At. Mol. Opt. Phys.* **35** 3937
[10] Spranger T and Kirchner T 2004 *J. Phys. B: At. Mol. Opt. Phys.* **37** 4159
[11] Schenk G and Kirchner T 2009 *J. Phys. B: At. Mol. Opt. Phys.* **42** 205202
[12] Galassi M E, Rivarola R D and Fainstein P D 2007 *Phys. Rev.* A **75** 052708
[13] Sigaud G M *et al* 2004 *Phys. Rev.* A **69** 062718
[14] Archubi C D, Montanari C C and Miraglia J E 2007 *J. Phys. B: At. Mol. Opt. Phys.* **40** 943
[15] Drescher M *et al* 2002 *Nature* **419** 803
[16] Cavalieri A L *et al* 2007 *Nature* **449** 1029
[17] Kazansky A K, Sazhina I P and Kabachnik N M 2009 *J. Phys. B: At. Mol. Opt. Phys.* **42** 245601
[18] Landers A L *et al* 2009 *Phys. Rev. Lett.* **102** 223001
[19] Morgan D V, Sagurton M and Bartlett R J 1997 *Phys. Rev.* A **55** 1113
[20] Saito N and Suzuki I H 1992 *Phys. Scr.* **45** 253
[21] Brünken S, Gerth Ch, Kanngieber B, Luhmann T, Richter M and Zimmermann P 2002 *Phys. Rev.* A **65** 042708
[22] Viefhaus J *et al* 2004 *Phys. Rev. Lett.* **92** 083001
[23] Tamenori Y, Okada K, Tanimoto S, Ibuki T, Nagaoka S, Fujii A, Haga Y and Suzuki I H 2004 *J. Phys. B: At. Mol. Opt. Phys.* **37** 117
[24] Armen G B, Kanter E P, Krässig B, Levin J C, Southworth S H and Young L 2004 *Phys. Rev.* A **69** 062710
[25] Hikosaka Y, Lablaniquie P, Penent F, Kaneyasu T, Shigemasa E, Eland J H D, Aoto T and Ito K 2007 *Phys. Rev.* A **76** 032708
[26] Hayaishi T, Yagishita T, Shigemasa E, Murakami E and Morioka Y 1990 *J. Phys. B: At. Mol. Opt. Phys.* **23** 4431
[27] Karmmerling B, Krassig B and Schmidt V 1992 *J. Phys. B: At. Mol. Opt. Phys.* **25** 3621
[28] Hayaishi T, Matsui T, Yoshii H, Higurashi A, Murakami E, Yagishita A, Aoto T, Onuma T and Morioka Y 2002 *J. Phys. B: At. Mol. Opt. Phys.* **35** 141
[29] Tamenori Y *et al* 2002 *J. Phys. B: At. Mol. Opt. Phys.* **35** 2799
[30] Hikosaka Y, Aoto T, Lablaniquie P, Penent F, Shigemasa E and Ito K 2006 *J. Phys. B: At. Mol. Opt. Phys.* **39** 3457
[31] Matsui T, Yoshii H, Tsukamoto K, Kawakita S, Murakami E, Adachi J, Yagishita A, Morioka Y and Hayaishi T 2004 *J. Phys. B: At. Mol. Opt. Phys.* **37** 3745

J. Phys. B: At. Mol. Opt. Phys. **43** (2010) 165201

C C Montanari *et al*

[32] Kirchner T, Gulyás L, Lüdde H J, Engel E and Dreizer R M 1998 *Phys. Rev. A* **58** 2063

[33] Kirchner T and Horbatsch M 2001 *Phys. Rev* A **63** 062718

[34] Tachino C A, Galassi M E and Rivarola R D 2008 *Phys. Rev. A* **77** 032714

[35] Miraglia J E and Gravielle M S 2008 *Phys. Rev. A* **78** 052705

[36] Miraglia J E 2009 *Phys. Rev. A* **79** 022708

[37] Salvat F, Fernandez-Varea J M and Williamson W Jr 1995 *Comput. Phys. Commun.* **90** 151

[38] Miraglia J E and Gravielle M S 2010 *Phys. Rev. A* **81** 042709

[39] Tachino C A, Galassi M E and Rivarola R D 2009 *Phys. Rev. A* **80** 014701

[40] Scully S W J, Wyer J A, Shah M B, Montenegro E C, Kimura M and Tawara H 2005 *Phys. Rev. A* **72** 030701

[41] Cavalcanti E G, Sigaud G M, Montenegro E C and Schmidt-Bocking H 2003 *J. Phys. B: At. Mol. Opt. Phys.* **36** 3087

[42] Sant'Anna M M, Luna H, Santos A C F, McGrath C, Shah M B, Cavalcanti E G, Sigaud G M and Montenegro E C 2003 *Phys. Rev. A* **68** 042707

[43] Kochur A G, Sukhorukov V L, Dudenko A I and Demekhin Ph V 1995 *J. Phys. B: At. Mol. Opt. Phys.* **28** 387

[44] Viefhaus J, Grum-Grzhimailo A N, Kabachnik N M and Becker U 2004 *J. Electron Spectrosc. Relat. Phenom.* **141** 121

[45] Hayaishi T, Murakami E, Yagishita A, Koike F, Morioka Y and Hansen J E 1988 *J. Phys. B: At. Mol. Opt. Phys.* **21** 3203

[46] Kanngieber B *et al* 2000 *Phys. Rev. A* **62** 014702

[47] Kochur A G, Dudenko A I, Sukhorukov V L and Petrov I D 1994 *J. Phys. B: At. Mol. Opt. Phys.* **27** 1709

[48] Hayaishi T, Murakami E, Morioka Y, Shigemasa E, Yagishita A and Koike F 1995 *J. Phys. B: At. Mol. Opt. Phys.* **28** 1411

[49] DuBois R D, Toburen L H and Rudd M E 1984 *Phys. Rev. A* **29** 70

[50] DuBois R D 1989 *Phys. Rev. A* **39** 4440

[51] Andersen L H, Hvelplund P, Knudsen H, Möller S P, Sörensen A H, Elsener K, Rensfelt K G and Uggerhöj E 1987 *Phys. Rev. A* **36** 3612

[52] Schram B L, Boerboom A J H and Kistermaker J 1966 *Physica* **32** 185

[53] Santos A C F, Melo W S, Sant'Anna M M, Sigaud G M and Montenegro E C 2001 *Phys. Rev. A* **63** 062717

[54] McCallion P, Shah M B and Gilbody H B 1992 *J. Phys. B: At. Mol. Opt. Phys.* **25** 1061

[55] Syage J A 1992 *Phys. Rev. A* **46** 5666